Galvanomagnetic Properties of a Nonellipsoidal Nonparabolic Band Model. II. Weak-Field Magnetoresistance*

C. C. Evans†
Wesleyan University, Middletown, Connecticut 06457 *and*
U.S. Naval Ordnance Laboratory, Silver Spring, Maryland 20910

and

T. A. Reglein and R. S. Allgaier
U.S. Naval Ordnance Laboratory, Silver Spring, Maryland 20910

(Received 1 December 1969)

The weak-field magnetoresistance is calculated for three cubically symmetric versions of Cohen's multivalley model (originally derived for Bi) in which the valleys are surfaces of revolution along the ⟨111⟩, ⟨100⟩, and ⟨110⟩ directions of momentum space. The Jones-Zener weak-field solution of the Boltzmann equation, an isotropic scattering time, and degenerate statistics are assumed. The Seitz coefficients b, c, and d and the symmetry parameter z ($b+c+zd=0$) were computed for about 3000 values of the energy and mass parameters ϵ and μ which cause the model to become nonellipsoidal and nonparabolic. Graphs of the results are presented for selected values of ϵ and μ. For $\mu=1$, the z values are precisely the same $(0, \pm 1)$ as in the corresponding ellipsoid-of-revolution parabolic models. Otherwise, $|z|$ deviates only slightly (<0.3) from the simple values for wide ranges of ϵ and μ, including the range in which the Fermi surface acquires a very distorted dumbbell shape. The only exception is a peak in z which occurs for $\mu<1$ when the energy surfaces are nearly isotropic and b, c, and d are all small. Experimental values of z in highly degenerate samples of p-type SnTe lie between -1 and -6, the coefficient b is large, and the Fermi surfaces in this compound are known to be strongly prolate and ⟨111⟩ oriented. Hence the Cohen model, when used with the above-mentioned restrictions, cannot account for the experimental weak-field magnetoresistance in SnTe. The significance of this result, as well as some modifications which might bring theory and experiment closer together, is discussed.

I. INTRODUCTION

This is a continuation of a study of galvanomagnetic effects in a nonellipsoidal nonparabolic model. The weak-field Hall coefficient R_0 was treated in an earlier paper[1] (hereafter called part I); the present work investigates the weak-field magnetoresistance and compares the results with experimental data on SnTe.[2]

The models used for the calculation are cubically symmetric versions of the one which Cohen derived for Bi.[3] This model was chosen because of the basic similarity between the band structures of the column-V semimetals As, Sb, and Bi, and IV–VI semiconductors such as PbS, PbSe, PbTe, and SnTe.[4] Furthermore, the Cohen model generates dumbbell-shaped Fermi surfaces for certain ranges of its parameters, and Shubnikov–de Haas measurements on SnTe had suggested the possibility of such a surface.[5]

The weak-field Hall coefficient may be written in the form

$$R_0 = r/ne, \tag{1}$$

where r is a dimensionless mixing or anisotropy factor[6] and ne is the charge density. Hall-coefficient measurements on p-type SnTe revealed that $r=(0.6\pm10)\%$ over a wide range of carrier densities.[7] The factor r lies between 0.75 and 1 for all cubically symmetric multivalley models composed of prolate ellipsoids of revolution. The results of paper I showed that, in general, the distortions of the Cohen surface lower the values of r, so that the model can easily account for the experimental Hall data on SnTe.

However, matching experimental and theoretical Hall-factor values does not provide very strong evidence for the suitability of a particular band model. Magnetoresistance behavior is much more sensitive to the details of the shape of a Fermi surface, and would provide a more severe test of any proposed model.

We wish to point out an error in the final expression for r found in Eq. (19) of paper I. A factor of K should be inserted between the first curly bracket and integral sign in the numerator. The correct expression was used to prepare Table I and Fig. 2 of that paper.

II. COHEN SURFACE

Cohen considered three types of Fermi surfaces in his paper on Bi.[3] His case (a) will be used

oriented along the ⟨111⟩, ⟨100⟩, and ⟨110⟩ directions of momentum space. In the first two cases, symmetry requires that the Cohen-type Fermi surface become a surface of revolution. The same shape was also used for the third case.

The Cohen surface of revolution is given by

$$\mathcal{E}=\frac{p_t^2}{2m_t}\,\frac{1}{1+(\mathcal{E}/\mathcal{E}_g)+(p_l^2/2m_l'\mathcal{E}_g)}+\frac{p_l^2}{2m_l}\ , \qquad (2)$$

where the momenta p_l and p_t identify the longitudinal (symmetry) axis and any transverse direction, respectively, m_l and m_t are the corresponding band-edge masses, $\mathcal{E}$ is the carrier energy, and $\mathcal{E}_g$ and m_l' are the two parameters which (when finite) make the model nonparabolic and nonellipsoidal, respectively.

The computation will be presented in terms of the dimensionless variables $\epsilon=\mathcal{E}/\mathcal{E}_g$, $\mu=m_l/m_l'$, $x^2=p_t^2/m_t\mathcal{E}_g$, and $y^2=p_l^2/m_l\mathcal{E}_g$. These substitutions reduce Eq. (2) to the more compact form

$$\epsilon=\tfrac{1}{2}x^2(1+\epsilon+\tfrac{1}{2}\mu y^2)^{-1}+\tfrac{1}{2}y^2\ . \qquad (3)$$

Deviations from parabolicity and ellipticity now result from *nonzero* values of ϵ and μ, respectively. Additional remarks about the nature of this Cohen surface of revolution are contained in Sec. 2 of paper I.

III. OUTLINE OF CALCULATION

A detailed description of the calculation is given in the thesis of the first author.[8] The calculation uses the Jones-Zener weak-field solution of the Boltzmann equation, and assumes degenerate statistics (which are appropriate for the high-carrier-density data on SnTe) and an isotropic scattering time τ. The effects that these restrictions have on the significance of the results will be discussed in Sec. IV.

The first step is to calculate the magnetoconductivity tensor components σ_{ijkl} in the expression

$$I_i=\sigma_{ij}E_j+\sigma_{ijk}E_jH_k+\sigma_{ijkl}E_jH_kH_l+\cdots \qquad (4)$$

for a single Cohen surface. Summation from 1 to 3 is implied wherever repeated indices appear in the above and in other equations to follow. The zero-field conductivity and Hall terms σ_{ij} and σ_{ijk} were worked out in paper I. In all cases, the results were obtained from the usual Jones-Zener iterative solution to the Boltzmann equation [see Eq. (9) in paper I].

Before any calculations are actually carried out, it is possible to establish certain relationships among the σ_{ijkl} which follow from Onsager's relation, or from the symmetry properties of the model, but not from the specific analytical form of the Cohen surface. To begin with the Cohen surface of revolution can be placed in an orthogonal coordinate system such that it has twofold rotational symmetry about each coordinate axis. Consequently, the only possible nonzero σ_{ijkl} components are three σ_{iiii}, six σ_{iijj}, and six $(\sigma_{ijij}+\sigma_{ijji})$. The last two types of terms are paired because they have no separate physical significance.

Furthermore, when axis 3 is taken as the axis of rotation (i.e., the p_l or y axis) of the Cohen surface, axes 1 and 2 become indistinguishable, and certain equalities among the nonzero σ_{ijkl} must hold. Use of Onsager's relation leads to further simplifications. As a result of the above, only the following seven components need be computed:

$$\sigma_{1111},\ \sigma_{3333}\ ,$$
$$\sigma_{1122},\ \sigma_{1133},\ \sigma_{3311}\ ,$$
$$(\sigma_{1212}+\sigma_{1221}),\ (\sigma_{1313}+\sigma_{1331})\ .$$

But there is one additional relationship among the σ_{ijkl}. Because the Cohen surface is a surface of revolution, *all* directions in the 1-2 plane are equivalent. Some simple algebra shows, as a consequence, that

$$\sigma_{1111}=\sigma_{1122}+\sigma_{1212}+\sigma_{1221}\ . \qquad (5)$$

Now we proceed to the calculation itself; it reveals that σ_{3333} and σ_{1331} are identically zero. The remaining terms have the form

$$\sigma_{ijkl}=(+\text{or}-)\,\frac{ne^4}{m_um_vm_w}\int_0^\infty\tau^3A_{ijkl}\epsilon^{3/2}\frac{\partial f_0}{\partial\epsilon}\,d\epsilon\Big/\int_0^\infty A_n\epsilon^{3/2}\frac{\partial f_0}{\partial\epsilon}\,d\epsilon\ . \qquad (6)$$

The appropriate signs and combinations of mass components m_t and m_l are shown in Table I. The functions A_{ijkl} are written out in the Appendix, $A_n=1+\epsilon(1+\frac{1}{5}\mu)$. For degenerate statistics, the ratio of integrals in Eq. (6) reduces to τ^3A_{ijkl}/A_n, evaluated at the Fermi energy.

The difference between the structure of the present results and those for an ellipsoidal parabolic model is the presence of nonzero σ_{1111} and σ_{1221} terms. The calculations also reveal that

$$\sigma_{1111}=-\sigma_{1221} \qquad (7)$$

and

$$3\sigma_{1111}=\sigma_{1122}+\sigma_{1313}\ . \qquad (8)$$

The latter equation is analogous to Eq. (10) in Zitter's analysis of Bi.[9]

The next step is to transform the results for each valley to the cubic-axis coordinate system of the crystal, and sum the contributions from all the valleys. The results, unlike those for the σ_{ij} and σ_{ijk} terms, depend on the valley orientations.

The final step is to invert the results and relate

TABLE I. Signs and mass combinations for the nonzero σ_{ijkl} of Eq. (6).

Component	Sign	Masses
σ_{1111}	−	$m_t^2 m_l$
σ_{1122}	−	$m_t^2 m_l$
σ_{1133}	−	m_t^3
σ_{3311}	−	$m_t m_l^2$
σ_{1212}	+	$m_t^2 m_l$
σ_{1313}	+	$m_t^2 m_l$

them to the magnetoresistance coefficients. We define a dimensionless weak-field magnetoresistance by the relation

$$\Delta\rho/\rho_0 = M_{\alpha\beta\gamma}^{\delta\epsilon\zeta}\,(\mu_H H/C)^2 \,, \tag{9}$$

where $\Delta\rho/\rho_0$ is the fractional change in the zero-field resistance, $\alpha\beta\gamma$ and $\delta\epsilon\zeta$ identify the current and magnetic field directions relative to the cubic axes of the crystal, μ_H is the Hall mobility, and H is the magnetic field intensity. The factor $C = 10^8$ when μ_H is in $\mathrm{cm^2/V\,sec}$ and H is in Oe.

For crystals having the three highest types of cubic symmetry ($m3m$, $\bar{4}3m$, and 432 in the abbreviated Hermann-Maugin notation), the weak-field magnetoresistance for all current and field directions may be expressed in terms of the three dimensionless Seitz coefficients

$$M_{\alpha\beta\gamma}^{\delta\epsilon\zeta} = b + c\,(\iota_s\eta_s)^2 + d(\iota_s^2\eta_s^2) \,, \tag{10}$$

where ι_s and η_s are the direction cosines of the sample current and magnetic field directions with respect to the cubic axes. We will also examine the expressions for the magnetoresistance symmetry parameter z, defined as

$$z = -(b+c)/d \,. \tag{11}$$

The final results for the three multivalley models are summarized below. They are expressed in terms of $K(=m_l/m_t)$, the A_{ij} and A_{ijk} given in Eq. (16) of paper I, and the A_{ijkl} defined by Eq. (6) and written out in the Appendix. Equations (5), (7), and (8) were used to eliminate σ_{1212}, σ_{1221}, and σ_{1313} from the results so that only the A_{ijkl} corresponding to σ_{1111}, σ_{1122}, σ_{1133}, and σ_{3311} appear:

⟨111⟩ model

$$b = \tfrac{1}{3}A(-5KA_{1111} + 5KA_{1122} + 2K^2A_{1133} + 2A_{3311}) - 1, \tag{12a}$$

$$c = -\tfrac{1}{3}A(-11KA_{1111} + 5KA_{1122} + 2K^2A_{1133} + 2A_{3311}) + 1, \tag{12b}$$

$$d = \tfrac{2}{3}A(5KA_{1111} - 2KA_{1122} + K^2A_{1133} + A_{3311}) \,, \tag{12c}$$

$$z = \frac{-3KA_{1111}}{5KA_{1111} - 2KA_{1122} + K^2A_{1133} + A_{3311}} \,; \tag{12d}$$

⟨100⟩ model

$$b = A(KA_{1122} + K^2A_{1133} + A_{3311}) - 1 \,, \tag{13a}$$

$$c = -A(-7KA_{1111} + 3KA_{1122}) + 1 \,, \tag{13b}$$

$$d = -A(5KA_{1111} - 2KA_{1122} + K^2A_{1133} + A_{3311}) \,, \tag{13c}$$

$$z = \frac{7KA_{1111} - 2KA_{1122} + K^2A_{1133} + A_{3311}}{5KA_{1111} - 2KA_{1122} + K^2A_{1133} + A_{3311}} \,; \tag{13d}$$

⟨110⟩ model

$$b = \tfrac{1}{4}A(-5KA_{1111} + 6KA_{1122} + 3K^2A_{1133} + 3A_{3311}) - 1, \tag{14a}$$

$$c = -\tfrac{1}{2}A(-9KA_{1111} + 4KA_{1122} + K^2A_{1133} + A_{3311}) + 1, \tag{14b}$$

$$d = \tfrac{1}{4}A(5KA_{1111} - 2KA_{1122} + K^2A_{1133} + A_{3311}) \,, \tag{14c}$$

$$z = \frac{-(13KA_{1111} - 2KA_{1122} + K^2A_{1133} + A_{3311})}{5KA_{1111} - 2KA_{1122} + K^2A_{1133} + A_{3311}} \,, \tag{14d}$$

where $A = (2KA_{11} + A_{33})/K(KA_{123} + 2A_{312})^2$. (15)

IV. DISCUSSION

It is to be emphasized that Eqs. (12)–(15) result when the Cohen model is substituted into the Jones-Zener solution of the Boltzmann equation, and it is assumed that the statistics are degenerate and the scattering time is isotropic. These results are functions of K, and (through the presence of the A_{ij}, A_{ijk}, and A_{ijkl}) of the two Cohen-model parameters ϵ the reduced energy and μ the interband mass ratio [see Eq. (3)]. When $\mu = 0$, the Fermi surface remains ellipsoidal at all ϵ, but its shape changes with energy. When $\mu \neq 0$, the Fermi surface is not ellipsoidal at any nonzero ϵ.

The symmetry parameter z has the values 0, +1, and −1 for ellipsoid-of-revolution parabolic (EORP) models with valleys in the ⟨111⟩, ⟨100⟩, and ⟨110⟩ directions, respectively. The present results differ from these simple values only because of the presence of A_{1111}. This is an example of Keyes's analysis which demonstrated that the simple values result whenever the sum of the three longitudinal magnetoconductivity components of a single valley (i.e., the σ_{iiii}) is zero.[10]

As in the case of the Hall coefficient [see Eqs. (23) and (24) of paper I], the results summarized in Eqs. (13)–(15) become considerably simpler when $\mu = 1$, even though the Fermi surfaces are *not* ellipsoidal in this case. For $\mu = 1$, $A_{1111} = 0$, so that the EORP values for the symmetry parameter z result. Also, $A_{1313} = A_{1122}$. We define $K' = XK$, where

$$X = (1 + \tfrac{6}{5}\epsilon)/(1 + \tfrac{12}{5}\epsilon + \tfrac{12}{7}\epsilon^2) \tag{16}$$

TABLE II. Calculated Seitz coefficients and symmetry parameters for cubically symmetric Cohen models with $\mu = 1$.

Model	b	c	d	z
⟨111⟩	$\frac{(2K'+1)(2K'^2+5K'+2W)}{3K'(K'+2)^2}-1$	$\frac{-(2K'+1)(2K'^2+5K'+2W)}{3K'(K'+2)^2}+1$	$\frac{2(2K'+1)(K'^2-2K'+W)}{3K'(K'+2)^2}$	0
⟨100⟩	$\frac{(2K'+1)(K'^2+K'+W)}{K'(K'+2)^2}-1$	$\frac{-3(2K'+1)}{(K'+2)^2}+1$	$\frac{-(2K'+1)(K'^2-2K'+W)}{K'(K'+2)^2}$	+1
⟨110⟩	$\frac{3(2K'+1)(K'^2+2K'+W)}{4K'(K'+2)^2}-1$	$\frac{-(2K'+1)(K'^2+4K'+W)}{2K'(K'+2)^2}+1$	$\frac{(2K'+1)(K'^2-2K'+W)}{4K'(K'+2)^2}$	−1

and $W = XA_{3311}/A_{1122}$

$$= \frac{X(1+\frac{18}{5}\epsilon+\frac{228}{35}\epsilon^2+\frac{24}{5}\epsilon^3)}{1+\frac{12}{5}\epsilon+\frac{12}{7}\epsilon^2} \quad . \qquad (17)$$

Then the results of Eqs. (12)–(15) reduce to those shown in Table II. Their form is exactly the same as that found for the corresponding EORP models, except that K' has replaced K and W has replaced unity.

An IBM 7090 computer was used to evaluate the A_{ij}, A_{ijk}, and A_{ijkl} for about 3000 combinations of μ and ϵ in the range between 0 and 100. The results were used to calculate b, c, d, and z for

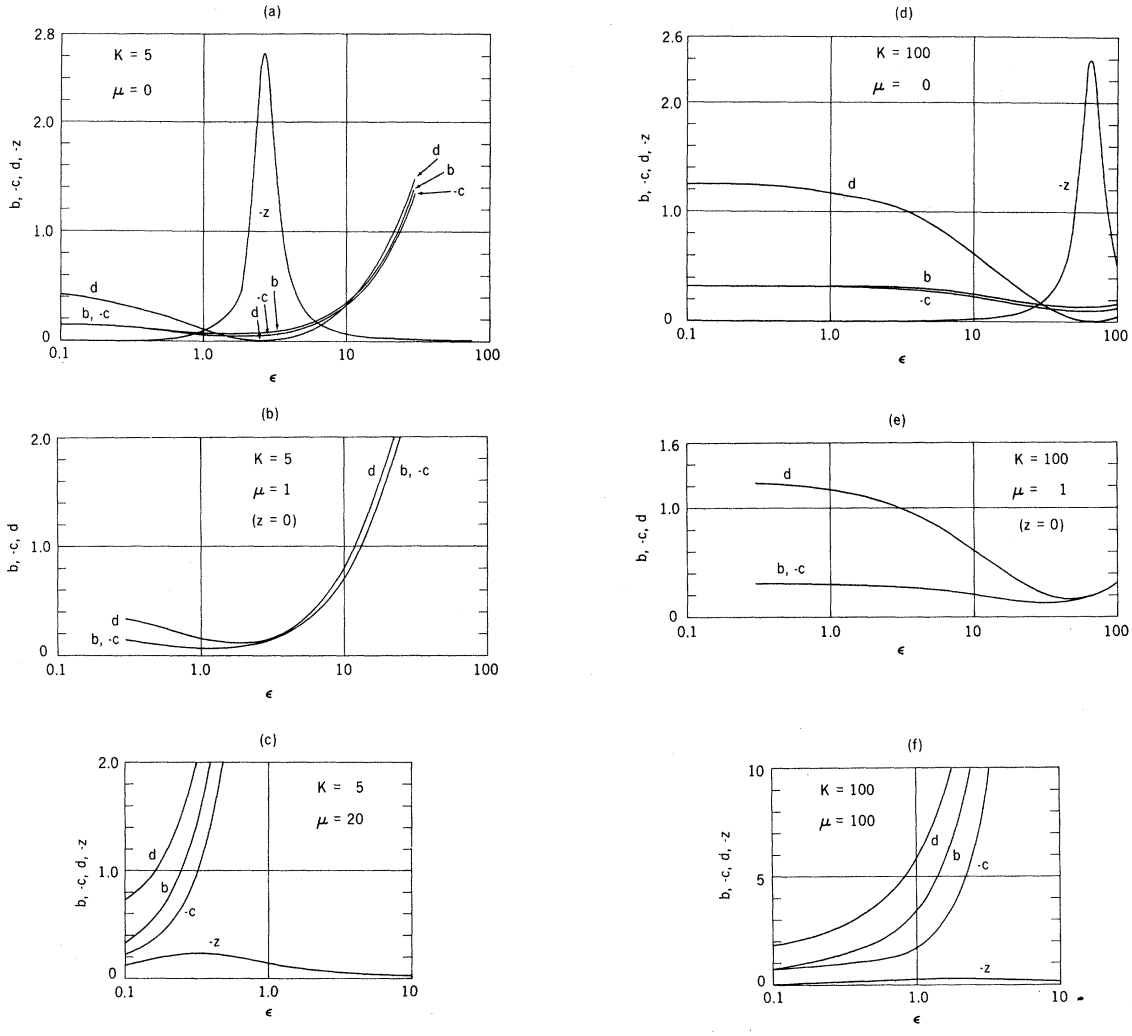

FIG. 1. Behavior of Seitz coefficients b, c, and d and magnetoresistance symmetry parameter z, as a function of energy ratio ϵ, for six combinations of mass ratios K and μ. All units are dimensionless.

the three multivalley models with $K = 5$, 10, 25, 50, and 100.

The behavior of b, c, d, and z as a function of ϵ, for selected values of μ and K in the $\langle 111 \rangle$ model, is shown in Fig. 1. This behavior is typical of the general results.

For $\epsilon = 0$, b, c, and d start out at the values which occur for the EORP model at that K value, since the Cohen model reduces to the simpler one at $\epsilon = 0$. As ϵ increases, b, c, and d decrease in magnitude and then increase again.

The explanation for this behavior is particularly straightforward when $\mu = 0$. Then the surfaces are always ellipsoidal, but they become less prolate, and ultimately oblate, with increasing ϵ. The coefficients b, c, and d are smallest near the ϵ value at which the Fermi surface becomes spherical. But they are not exactly zero, as they would be for an isotropic model and degenerate statistics. The reason is that the various derivatives on the surface are not isotropic because the shape of the Fermi surface changes with energy.

It is convenient to discuss the behavior of the symmetry parameter z in the ranges $\mu < 1$ and $\mu > 1$. For the $\langle 111 \rangle$ model, we have $z = 0$ at $\mu = 1$, as already noted (Table II), for all ϵ.

As μ goes from 1 to 0, a peak develops in z, occurring near the value $\epsilon \approx K - 1$. All of the coefficients b, c, and d have become small at this ϵ because the Fermi surface is nearly isotropic. The symmetry parameter becomes large simply because d is even smaller than $b + c$ [Eq. (11)], but only over a limited range of ϵ. It should be emphasized that the range $0 < \mu < 1$ corresponds to modestly distorted Fermi surfaces for all ϵ; no dumbbell shapes can develop [Eq. (5) of I].

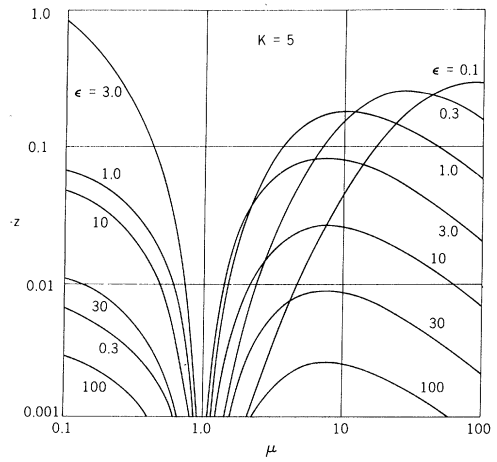

FIG. 2. Behavior of magnetoresistance symmetry parameter z as a function of mass ratio μ, for seven values of energy ratio ϵ, with mass ratio $K = 5$. All units are dimensionless.

TABLE III. Experimental weak-field magnetoresistance, Seitz coefficients, and symmetry parameters for p-type PbTe and SnTe.

Compound	PbTe		SnTe		SnTe	
Carrier density (10^{18} cm^{-3})	3		50		90	
Temperature (°K)	295	77	295	77	295	77
M_{110}^{110}	0.275	0.196	0.46	0.57	0.69	1.00
M_{110}^{001}	0.345	0.151	0.56	0.58	0.86	1.13
$M_{110}^{1\bar{1}0}$	0.605	0.348	0.72	0.66	1.04	1.20
b	0.345	0.151	0.56	0.58	0.86	1.13
c	−0.330	−0.152	−0.27	−0.10	−0.35	−0.20
d	0.520	0.394	0.34	0.16	0.36	0.15
z	−0.03	0.003	−0.9	−3.0	−1.4	−6.2

For $\mu > 1$, the Fermi surface becomes very distorted as ϵ increases, especially for large μ. This leads to large values of b, c, and d. Note particularly Fig. 1(f): All three coefficients exceed 10 before ϵ reaches 4. Nevertheless, the symmetry parameter only deviates from zero by modest amounts, viz., $|z|_{max} \approx 0.2$ and 0.3 for $\mu = 20$, $K = 5$ and for $\mu = 100$, $K = 100$, respectively. Figure 2 provides a more general indication of the behavior of z for $K = 5$ in the $\langle 111 \rangle$ model.

V. APPLICATION TO SnTe.

The motivation for carrying out this rather involved calculation was the hope that it could explain the very strange magnetoresistance data which had been obtained on SnTe.[2] A brief comparison of experiment and calculation was presented earlier.[11] Measured weak-field coefficients for SnTe at two temperatures and two carrier densities, together with values of b, c, d, and z derived from these data, are given in Table III. For comparison, the same quantities for p-type PbTe at a considerably lower carrier density are also included.[12]

As noted in the Introduction, the Cohen model was chosen for the calculation because it was appropriate in a general sense for IV–VI compounds, and, more specifically, because there seemed to be some experimental evidence for the dumbbell-shaped Fermi surface which was a feature of the model.

But the Cohen surface was then fed into the Jones-Zener solution of the Boltzmann equation, which is not a general solution of the Boltzmann equation. This type of solution might be quite unsuitable for the model under consideration. Since magnetoresistance is usually very sensitive to details of the behavior of electrons in electric and magnetic fields, a better solution to Boltzmann's equation might completely change the nature of the results embodied in Eqs. (12)–(15). This limitation must be kept in mind in any comparison of

theory and experiment.

On the other hand, we have the following historical facts pertaining specifically to multivalley models.[13] The special values of the magnetoresistance symmetry parameter z which were predicted by theory for cubically symmetric EORP multivalley models were obtained using the Jones-Zener solution to the Boltzmann equation. They were shown to apply if τ is isotropic, or if it is a tensor which is diagonal in the principal-axis coordinate system of each valley.

Experimentally, the predicted values have been confirmed ($z = 0$ in n-type Ge, a $\langle 111 \rangle$ model, and $z = 1$ in n-type Si, a $\langle 100 \rangle$ model) over wide temperature ranges in which isotropic scattering, anisotropic scattering, or mixtures of both are known to be appropriate.

As shown in Table III, the experimental weak-field magnetoresistance symmetry in p-type PbTe is very close to the $z = 0$ value predicted for a $\langle 111 \rangle$ EORP model. More direct measurements (using the Shubnikov–de Haas effect) of the Fermi surfaces near the top of the valence band in PbTe confirm that they are prolate, $\langle 111 \rangle$-oriented ellipsoids.[14] The scattering in p-type PbTe is not isotropic, since the K values deduced from the strong- and weak-field data differ by more than a factor of 2.

Because the EORP multivalley model, assuming a Jones-Zener-type solution and an isotropic τ, works so well for PbTe, it seemed reasonable to apply a generalized multivalley model with the same assumptions to SnTe.

As shown in Table III, z in SnTe is far from the zero value found in PbTe, and, furthermore, it depends strongly on temperature and carrier density. Since the z values in SnTe are negative and, at room temperature, not too different from -1, we at one time considered that some kind of generalization of a $\langle 110 \rangle$ EORP model might be appropriate.

But it is now definitely established that the Fermi surfaces in p-type SnTe are strongly prolate and $\langle 111 \rangle$ oriented.[15] Hence the suitability of the Cohen model must be based on the calculated results for the $\langle 111 \rangle$ version only, i.e., on Eqs. (12).

The only region in which we could hope to match the z values of this $\langle 111 \rangle$ version to the experimental results is near the peaks which occur in z when $\mu < 1$. But this region corresponds to a nearly isotropic surface and to values of b, c, and d which are all small. These properties are completely different from the weak-field results shown in Table III and from the strong-field data which provided the information about the Fermi-surface shape.[15]

We feel that it is particularly significant that the calculated z values deviate so slightly from the results for the simpler EORP models over such a wide range of parameters of the Cohen model. In most cases, these parameter values correspond to a highly distorted Fermi surface which is rapidly changing its shape as a function of energy.

This shape-evolution feature alters the relative values of the Fermi velocity on different parts of the Fermi surface. Since the Fermi velocity and scattering time occur in combination in the various transport integrals, the presence of shape evolution is equivalent to the introduction of τ anisotropy.[16] The anisotropy must be of a polar, not an azimuthal nature; i.e., it must be consistent with the rotational symmetry of the valleys.

It therefore seems quite likely that if the results for the Cohen model were recalculated, assuming this kind of anisotropic τ, they would still predict only modest deviations from the magnetoresistance symmetry of the corresponding EORP models.

VI. CONCLUSIONS

Some of the high-field measurements on SnTe had suggested that the Fermi surfaces might have a dumbbell shape.[5] It therefore seemed quite possible that the Cohen model, for some range of its parameters, could reproduce the large deviations of the magnetoresistance symmetry from the usual value for the $\langle 111 \rangle$ EORP model.

This hope was not realized. Instead we are led to the tentative conclusion that magnetoresistance symmetry is generally insensitive to distortions from ellipsoidal multivalley models, whether they involve mass or scattering anisotropy, *provided* that the rotational invariance of the carrier properties in each valley is preserved.

Hence it appears that this rotational invariance is not appropriate for SnTe. For example, the cross sections of the Fermi surface perpendicular to the $\langle 111 \rangle$ symmetry axis of the valley could develop three- or sixfold symmetry.

Unfortunately, such distorted Fermi surfaces will usually require so many parameters to specify them that numerous alternative types of surfaces of similar complexity could equally well account for the experimental results. This is the point at which weak-field magnetoresistance will no longer be a useful tool for acquiring insight into the behavior of carriers in crystals.

This point may have been reached in SnTe. We believe that the experimental data are accurate, and are characteristic of high-quality homogeneous material. But we have been unable to relate the observed behavior to any of the models which have been suggested by calculations or by other types of experimental data on SnTe.

APPENDIX: FUNCTIONS A_{ijkl}

Only A_{1111}, A_{1122}, A_{1133}, and A_{3311} will be given. Eqs. (5), (7), and (8) may be used to obtain A_{1221}, A_{1212}, and A_{1313}:

$$A_{1111} = -\tfrac{3}{4} D_1[a^2 L_4^0 - 2ab L_4^2 + (b^2 - 2\mu\epsilon a) L_4^4 + 2\mu\epsilon b L_4^6 + \mu^2\epsilon^2 L_4^8] - \tfrac{9}{2} D_2[\tfrac{1}{3} a^2 L_5^2 - \tfrac{2}{5} ab L_5^4 + \tfrac{1}{7}(b^2 - 2\mu\epsilon a) L_5^6 + \tfrac{2}{9}\mu\epsilon b L_5^8 + \tfrac{1}{11}\mu^2\epsilon^2 L_5^{10}] , \quad \text{(A1)}$$

$$A_{1122} = \tfrac{3}{2} D_0[ab L_3^0 + \tfrac{1}{3}(6\mu\epsilon a - b^2) L_3^2 - \tfrac{7}{5}\mu\epsilon b L_3^4 - \tfrac{6}{7}\mu^2\epsilon^2 L_3^6] - \tfrac{3}{4} D_1[3a^2 L_4^0 - \tfrac{22}{3} ab L_4^2 + \tfrac{19}{5}(b^2 - 2\mu\epsilon a) L_4^4 + \tfrac{54}{7}\mu\epsilon b L_4^6 + \tfrac{35}{9}\mu^2\epsilon^2 L_4^8] - \tfrac{27}{2} D_2[\tfrac{1}{3} a^2 L_5^2 - \tfrac{2}{5} ab L_5^4 + \tfrac{1}{7}(b^2 - 2\mu\epsilon a) L_5^6 + \tfrac{2}{9}\mu\epsilon b L_5^8 + \tfrac{1}{11}\mu^2\epsilon^2 L_5^{10}] , \quad \text{(A2)}$$

$$A_{1133} = \tfrac{3}{2} D_0(a L_3^0 - \tfrac{1}{3} b L_3^2 - \tfrac{1}{5}\mu\epsilon L_3^4), \quad \text{(A3)}$$

$$A_{3311} = D_0[(b^3 - 6\mu\epsilon ab) L_3^2 - \tfrac{12}{5}\mu\epsilon(3\mu\epsilon a - 4b^2) L_3^4 + \tfrac{138}{7}\mu^2\epsilon^2 b L_3^6 + 12\mu^3\epsilon^3 L_3^8] - 6 D_1[\tfrac{2}{3} ab^2 L_4^2 + \tfrac{1}{5}(14\mu\epsilon ab - 3b^3) L_4^4 + \tfrac{2}{7}\mu\epsilon(10\mu\epsilon a - 11 b^2) L_4^6 - \tfrac{46}{9}\mu^2\epsilon^2 b L_4^8 - \tfrac{28}{11}\mu^3\epsilon^3 L_4^{10}] - 18 D_2[\tfrac{1}{5} ab^2 L_5^4 + \tfrac{1}{7}(4\mu\epsilon ab - b^3) L_5^6 + \tfrac{1}{9}\mu\epsilon(4\mu\epsilon a - 5b^2) L_5^8 - \tfrac{8}{11}\mu^2\epsilon^2 b L_5^{10} - \tfrac{4}{13}\mu^3\epsilon^3 L_5^{12}] , \quad \text{(A4)}$$

where $a = (1 + \epsilon)$, $b = 1 + \epsilon(1 - \mu)$,

and $D_n = (1 - \mu)^n \epsilon^n / (1 + 2\epsilon)^{n+3}$.

The function L_α^β are defined, and some members of the set are written out in Appendix B of paper I Additional members needed for Eqs. (A1)–(A4) are

$$L_4^0 = \tfrac{1}{48}[8/(1+w)^3 + 10/(1+w)^2 + 15/(1+w) + 15 L_1^0],$$

$$L_4^2 = \tfrac{3}{48}[-8/(1+w)^3 + 2/(1+w)^2 + 3/(1+w) + 3 L_1^0]/w,$$

$$L_4^4 = \tfrac{5}{48}[8/(1+w)^3 - 14/(1+w)^2 + 3/(1+w) + 3 L_1^0]/w^2,$$

$$L_4^6 = \tfrac{7}{48}[-8/(1+w)^3 + 26/(1+w)^2 - 33/(1+w) + 15 L_1^0]/w^3 ,$$

$$L_4^8 = \tfrac{9}{48}[8/(1+w)^3 - 38/(1+w)^2 + 87/(1+w) - 105 L_1^0 + 48]/w^4 ,$$

$$L_4^{10} = \tfrac{11}{48}[-8/(1+w)^3 + 50/(1+w)^2 - 165/(1+w) + 315 L_1^0 - 192 + \tfrac{48}{3} w]/w^5,$$

$$L_5^0 = \tfrac{1}{384}[48/(1+w)^4 + 56/(1+w)^3 + 70/(1+w)^2 + 105/(1+w) + 105 L_1^0] ,$$

$$L_5^2 = \tfrac{3}{384}[-48/(1+w)^4 + 8/(1+w)^3 + 10/(1+w)^2 + 15/(1+w) + 15 L_1^0]/w ,$$

$$L_5^4 = \tfrac{5}{384}[48/(1+w)^4 - 72/(1+w)^3 + 6/(1+w)^2 + 9/(1+w) + 9 L_1^0]/w^2 ,$$

$$L_5^6 = \tfrac{7}{384}[-48/(1+w)^4 + 136/(1+w)^3 - 118/(1+w)^2 + 15/(1+w) + 15 L_1^0]/w^3 ,$$

$$L_5^8 = \tfrac{9}{384}[48/(1+w)^4 - 200/(1+w)^3 + 326/(1+w)^2 - 279/(1+w) + 105 L_1^0]/w^4 ,$$

$$L_5^{10} = \tfrac{11}{384}[-48/(1+w)^4 + 264/(1+w)^3 - 630/(1+w)^2 + 975/(1+w) - 945 L_1^0 + 384]/w^5 ,$$

$$L_5^{12} = \tfrac{13}{384}[48/(1+w)^4 - 328/(1+w)^3 + 1030/(1+w)^2 - 2295/(1+w) + 3465 L_1^0 - 1920 + (384/3)w]/w^6, \quad \text{(A5)}$$

where $w = (\mu - 1)\epsilon/(1 + 2\epsilon)$.

---

*Portions of this work constitute the thesis of C. C. Evans accepted by Wesleyan University in partial fulfillment of the requirements for the M. A. degree. This work was partially supported by ONR Contract No. PO-9-0163.

†Present address: 6 Saratoga Road, Auburn, Mass. 01501.

[1]R. S. Allgaier, Phys. Rev. 152, 808 (1966).

[2]R. S. Allgaier and B. B. Houston, Bull. Am. Phys. Soc. 7, 331 (1962); R. S. Allgaier, C. C. Evans, and B. B. Houston, *ibid.* 9, 646 (1964).

[3]M. H. Cohen, Phys. Rev. 121, 387 (1961).

[4]M. H. Cohen, L. M. Falicov, and S. Golin, IBM J. Res. Develop. 8, 215 (1964).

[5]J. R. Burke, R. S. Allgaier, B. B. Houston, J. Babiskin, and P. G. Siebenmann, Phys. Rev. Letters 14, 360 (1965).

[6]R. S. Allgaier, Phys. Rev. 165, 775 (1968).

[7]B. B. Houston, R. S. Allgaier, J. Babiskin, and P. G. Siebenmann, Bull. Am. Phys. Soc. 9, 60 (1964).

[8]C. C. Evans, M. A. thesis, Wesleyan University, 1965 (unpublished).

[9]R. N. Zitter, Phys. Rev. 127, 1471 (1962).

[10]R. W. Keyes, Phys. Rev. 111, 34 (1958).

[11]R. S. Allgaier, C. C. Evans, and T. A. Reglein, Bull. Am. Phys. Soc. 13, 431 (1968).

[12]R. S. Allgaier, Phys. Rev. 119, 554 (1960).

[13]A. C. Beer, *Galvanomagnetic Effects in Semiconductors* (Academic, New York, 1963), Chap. 8.

[14]J. R. Burke, B. B. Houston, H. T. Savage, J. Babiskin, and P. G. Siebenmann, Bull. Am. Phys. Soc. 13, 485 (1968); J. R. Burke Phys. Rev. (to be published).

[15]J. R. Burke, B. B. Houston, H. T. Savage, J. Babiskin, and P. G. Siebenmann, Phys. Soc. Japan Suppl. 21, 384 (1966).
[16]R. S. Allgaier (unpublished).

PHYSICAL REVIEW B VOLUME 2, NUMBER 4 15 AUGUST 1970

High-Field Conductivity of the ⟨111⟩ Valleys of Ge

W. P. Dumke
IBM *Watson Research Center, Yorktown Heights, New York* 10598
(Received 6 February 1970)

We have calculated the distribution function and drift velocity of electrons in the ⟨111⟩ valleys of Ge. The model used is essentially a one-valley model for an electric field in the [100] direction and without any electron transfer to higher valleys. The nonparabolicity of the conduction band and the nonclassical occupation of the acoustic modes are taken into account. The coupling constants were obtained from a fit to the low-field mobility, and because of the inclusion of nonparabolicity, the optical-mode coupling was smaller than previously used. The calculated drift velocity is in excellent agreement with the results of Ruch and Kino, and shows a low-temperature negative resistance which vanishes at somewhat above 77 °K. Although the electron energies at an electric field of several thousand V/cm indicate that some electron transfer to higher valleys is probably taking place, it is likely that this transfer is not primarily responsible for the observed negative resistance, but rather results in the resumption of a positive conductivity at still higher electric fields.

I. INTRODUCTION

The discovery of current oscillations in n-type Ge by McGroddy and Nathan[1] and the subsequent observation of a negative resistance in the bulk I-V characteristics[2,3] have resulted in a renewed interest in the electrical conductivity of Ge.

In comparison with the negative conductance observed in the I-V characteristics of GaAs, the negative conductance in Ge with the electric field along a ⟨100⟩ direction is relatively small and decreases with increasing temperature, vanishing at somewhat above 100 °K.

Theoretically, the conductivity properties of n-type Ge and GaAs should differ significantly in detail, since they depend upon features of the band structure and upon scattering mechanisms which are considerably different in the two materials. In GaAs, with its dominant polar optical-mode electron scattering mechanism, the drift velocity of electrons in the central minimum shows little tendency to reach a limiting value for electric fields at which electron transfer is unimportant. At higher fields (>3000 V/cm) electrons increasingly transfer to states in the ⟨100⟩ minima which have a considerably greater density of states than in the lowest conduction minimum and a much lower mobility. The electron transfer mechanism, therefore, acts rather effectively to produce a negative resistance in GaAs.

In Ge, electron transfer is also possible, but the effect on the electrical conductivity should be less drastic than in GaAs, because the densities of states and drift velocities of the upper and lower minima are not greatly different in Ge. In Ge, however, which is nonpolar, the drift velocity would be expected, under certain assumptions,[4] to reach a limiting value without electron transfer, so that even a small modification of the I-V characteristics due to transfer could cause a negative resistance.

The assumptions which yield a limiting drift velocity in Ge are not exactly obeyed, and it is important to accurately know the drift velocity of the electrons in the lowest minima if we are to understand the over-all I-V characteristics. In spite of some transfer to the ⟨100⟩ valleys, the electrons in the ⟨111⟩ valleys probably constitute a majority of the carriers over most of the negative-resistance region of interest.

The pressure experiment of Melz and McGroddy[5] is, in fact, qualitatively consistent with the model whereby the negative resistance in Ge is removed rather than produced by electron transfer to higher valleys. They found that the reduction by hydrostatic pressure of the separation between the ⟨111⟩ and ⟨100⟩ valleys was accompanied by a decrease in the amplitude of oscillations and an increase in